01 Jan 2004

An Integral Form of the Variational Nodal Method

M. A. Smith

G. Palmiotti

E. E. Lewis

Nicholas Tsoulfanidis
Missouri University of Science and Technology

Recommended Citation

M. A. Smith et al., "An Integral Form of the Variational Nodal Method," *Nuclear Science and Engineering*, vol. 146, no. 2, pp. 141 - 151, Taylor and Francis Group; Taylor and Francis; American Nuclear Society, Jan 2004.
The definitive version is available at https://doi.org/10.13182/NSE146-141

Nuclear Science and Engineering

ISSN: 0029-5639 (Print) 1943-748X (Online) Journal homepage: www.tandfonline.com/journals/unse20

An Integral Form of the Variational Nodal Method

M. A. Smith, G. Palmiotti, E. E. Lewis & N. Tsoulfanidis

To cite this article: M. A. Smith, G. Palmiotti, E. E. Lewis & N. Tsoulfanidis (2004) An Integral Form of the Variational Nodal Method, Nuclear Science and Engineering, 146:2, 141-151, DOI: 10.13182/NSE146-141

To link to this article: https://doi.org/10.13182/NSE146-141

Published online: 28 Jul 2017.

NUCLEAR SCIENCE AND ENGINEERING: **146**, 141–151 (2004)

An Integral Form of the Variational Nodal Method

M. A. Smith* and G. Palmiotti

Argonne National Laboratory
9700 South Cass Avenue
Argonne, Illinois 60439

E. E. Lewis

Northwestern University
Department of Mechanical Engineering
Evanston, Illinois 60208

and

N. Tsoulfanidis

University of Missouri, Rolla
Department of Nuclear Engineering
Rolla, Missouri 65409

Received December 4, 2002
Accepted April 25, 2003

Abstract—*An integral form of the variational nodal method is formulated, implemented, and tested. The method combines an integral transport treatment of the even-parity flux within the spatial node with an odd-parity spherical harmonics expansion of the Lagrange multipliers at the node interfaces. The response matrices that result from this formulation are compatible with those in the VARIANT code at Argonne National Laboratory. Spatial discretization within each node allows for accurate treatment of homogeneous or heterogeneous node geometries. The integral method is implemented in Cartesian x-y geometry and applied to three benchmark problems. The method's accuracy is compared to that of the standard spherical harmonic formulation of the variational nodal method, and the CPU and memory requirements of the two approaches are compared and contrasted. In general, for calculations requiring higher-order angular approximations, the integral method yields solutions with comparable accuracy while requiring substantially less CPU time and memory than the spherical harmonics approach.*

I. INTRODUCTION

Diffusion calculations based on nodal methods have long been a mainstay for performing whole-core thermal reactor analysis. Building on their success, nodal transport methods have been developed to treat fast reactor cores in which steeper flux gradients and increased leakage resulted in unacceptable errors in diffusion theory.[1–3] In both diffusion and transport methods, standard practice has been to homogenize cross sections and obtain response matrices for fuel assembly–sized nodal volumes. Experience with the variational nodal method implemented in the VARIANT code at Argonne National Laboratory, however, has indicated that refining the angular approximation in whole-core transport calculations beyond a P_5 spherical harmonic approximation provides only marginal improvements in accuracy when fuel assembly homogenization has been employed.[4,5] Other than increasing the number of energy groups, further refinement of the phase-space treatment of the Boltzmann transport equation requires more explicit representation of the spatial flux dependence

*E-mail: masmith@ra.anl.gov

within the fuel assemblies. Such refinements may be achieved by using heterogeneous node formulations (i.e., nodes containing cross-section discontinuities), using smaller node sizes, or a combination of both.

The treatment of heterogeneous nodes within the variational nodal framework thus far has been carried out in two separate approaches. In the first, higher-order polynomial trial functions were employed, and cross-section discontinuities were handled by precise spatial integration of the material heterogeneities.[6] In the second approach, a finite element approximation was employed, and cross-section discontinuities were allowed at finite element interfaces. Since each spatial node in VARIANT may itself be considered a hybrid finite element, the implementation of the finite element approximation within each node is referred to as the subelement form of the variational nodal method.[7–9]

To date, the subelement formulation has been implemented in two ways. In the first,[7] the fuel assembly is retained as the node size, and square subelements are used to represent individual homogenized fuel pin cells within each fuel assembly. In the second,[8,9] the node size is reduced to the size of a single fuel pin cell, and triangular finite elements are used to represent the fuel-coolant interface explicitly. Consistency in the level of phase-space approximation requires the use of finer energy group structures and higher-order angular approximations when fuel-coolant homogenization is eliminated. For example, spherical harmonic approximations as high as P_{21} have been required to obtain close agreement with reference Monte Carlo solutions for lattices containing heterogeneous MOX pin cells.[4] With large problem geometries, the high levels of refinement in space-angle approximations frequently lead to prohibitive CPU time and memory requirements.[8,9]

In this work we formulate an integral form of the variational nodal method that offers an alternative treatment of the angular variables for problems in which very refined angular approximations are required. The new formulation draws on earlier work[10] in which an integral transport method was applied to the even-parity transport equation. Now, however, we combine the integral treatment of the even-parity flux within the node with odd-parity spherical harmonic expansions of the Lagrange multipliers along the node interfaces. This integral approach can be employed in combination with either the orthogonal polynomial or finite subelement spatial discretization of the even-parity flux and leads to response matrices that are compatible with the VARIANT code.

In Sec. II we provide the details of the new formulation. In Sec. III we apply the method to three two-dimensional benchmark problems. The first is a fixed-source deep-penetration problem while the second is a three-region criticality problem. Both are treated using homogeneous nodes with orthogonal polynomial trial functions. The third problem is an Organisation of Economic Co-operation and Development (OECD) small-core mixed-oxide (MOX) benchmark, the heterogeneities of which are treated using the finite subelement formulation. For each of the three problems, the accuracy of the integral method is compared to that of the standard spherical harmonics formulation of the variational nodal method. Additionally, CPU and memory requirements of the two angular treatments are compared. We conclude in Sec. IV with a brief discussion of future research using the new formulation.

II. THEORY

The within-group formulation for the integral transport approach is derived from the same functional used in earlier forms of the variational nodal method.[3,4,7,9,11] After decomposing the problem domain into subdomains V_v (called nodes), the functional may be written as a superposition of nodal contributions:

$$F[\psi^+,\psi^-] = \sum_v F_v[\psi^+,\psi^-] \ , \tag{1}$$

with

$$F_v[\psi^+,\psi^-] = \int_v dV \Bigg\{ \int d\Omega [\Sigma_t^{-1}(\hat{\Omega}\cdot\vec{\nabla}\psi^+)^2 + \Sigma_t \psi^{+^2}] - \Sigma_s \phi^2 - 2\phi S \Bigg\} + 2\sum_\gamma \int_{\Gamma_\gamma} d\Gamma \int d\Omega \, \hat{n}_\gamma \cdot \hat{\Omega} \psi^+ \psi_\gamma^- \ . \tag{2}$$

Each node is bounded by an interface Γ broken into γ surfaces, Γ_γ, each with an outward normal $\hat{n}_\gamma$. The even- and odd-parity fluxes are denoted by $\psi^\pm(\vec{r},\hat{\Omega})$, the scalar flux by $\phi(\vec{r})$, and the group source by $S(\vec{r})$, where $\vec{r}$ is the spatial coordinate vector and $\hat{\Omega}$ is the direction of neutron travel. The total and within-group scattering cross sections are $\Sigma_t(\vec{r})$ and $\Sigma_s(\vec{r})$, and isotropic scattering and sources are assumed. The surface terms contain $\psi^-(\vec{r},\hat{\Omega})$, the odd-parity Lagrange multiplier that imposes continuity conditions across nodal interfaces.

Within each node the even-parity flux is approximated by a vector $\mathbf{f}(\vec{r})$ of known spatial trial functions and a vector of coefficients, $\zeta(\hat{\Omega})$, that is a function of angle:

$$\psi^+(\vec{r},\hat{\Omega}) = \mathbf{f}^T(\vec{r})\zeta(\hat{\Omega}) \ . \tag{3}$$

The scalar flux is thus approximated by

$$\phi(\vec{r}) = \mathbf{f}^T(\vec{r})\boldsymbol{\phi} \ , \tag{4}$$

where

$$\boldsymbol{\phi} = \int d\Omega \, \zeta(\hat{\Omega}) \ . \tag{5}$$

The Lagrange multiplier along each nodal interface Γ_γ is expanded in odd-parity spherical harmonics $\mathbf{k}_\gamma(\hat{\Omega})$ and spatial trial functions $\mathbf{h}_\gamma(\vec{r})$:

$$\psi^-(\vec{r},\hat{\Omega}) = \mathbf{k}_\gamma^T(\hat{\Omega}) \otimes \mathbf{h}_\gamma^T(\vec{r})\boldsymbol{\chi}_\gamma \ , \quad \vec{r} \in \Gamma_v \ , \tag{6}$$

where $\otimes$ indicates Kronecker tensor multiplication and $\boldsymbol{\chi}_\gamma$ is the vector of unknown coefficients.

For the spatial distribution of the even-parity flux, $\mathbf{f}(\vec{r})$, either the orthogonal polynomial representation or the finite element approximation may be used. The interface trial functions $\mathbf{h}_\gamma(\vec{r})$ are taken to be the same orthogonal polynomials as those employed in the VARIANT code. A point of departure between the spherical harmonic formulation in VARIANT and the new integral formulation is in the definition of $\mathbf{k}_\gamma(\hat{\Omega})$. For two-dimensional geometries, the integral formulation utilizes a complete set of odd-parity spherical harmonics through order N, while the spherical harmonics approach deletes $(N+1)/2$ odd-parity terms. Both formulations are defined such that they satisfy Rumyantsev interface conditions[11] as required for a nodal spherical harmonic method.

Inserting Eqs. (3), (4), and (6) into Eq. (2) yields the angularly dependent functional

$$F_v[\zeta,\boldsymbol{\chi}] = \int d\Omega \left[\zeta^T(\hat{\Omega})\mathbf{A}(\hat{\Omega})\zeta(\hat{\Omega}) - 2\boldsymbol{\phi}^T\mathbf{F}_s\boldsymbol{\phi} - 2\boldsymbol{\phi}^T\mathbf{s} + 2\sum_\gamma \zeta^T(\hat{\Omega})\mathbf{E}_\gamma(\hat{\Omega})\boldsymbol{\chi}_\gamma \right] , \tag{7}$$

where

$$\mathbf{A}(\hat{\Omega}) = \sum_K \sum_L \Omega^K\Omega^L\mathbf{P}^{K,L} + \mathbf{F}_t \tag{8}$$

$$\mathbf{E}_\gamma(\hat{\Omega}) = \hat{\Omega}\cdot\hat{n}_\gamma\mathbf{k}_\gamma^T(\hat{\Omega}) \otimes \mathbf{D}_\gamma \tag{9}$$

Ω^K, Ω^L = direction cosines of $\hat{\Omega}$.

The arrays of spatial matrices and the spatial source appearing in Eqs. (7), (8), and (9) are given by

$$P_{i,j}^{K,L} = \int dV [\nabla_K f_i(\vec{r})] \frac{1}{\Sigma_t(\vec{r})} [\nabla_L f_j(\vec{r})] \ , \tag{10}$$

$$F_{x,i,j} = \int dV f_i(\vec{r})\Sigma_x(\vec{r})f_j(\vec{r}) \ , \tag{11}$$

$$D_{\gamma,i,j} = \int_\gamma d\Gamma \, f_i(\vec{r})h_{\gamma,j}(\vec{r}) \ , \tag{12}$$

$$s_i = \int dV f_i(\vec{r})S(\vec{r}) \ , \tag{13}$$

and

$$\nabla_K = \partial/\partial x \ (K=1) \text{ and } \partial/\partial y \ (K=2) \ .$$

We require the functional in Eq. (7) to be stationary with respect to arbitrary variations in the vector $\zeta(\Omega)$. The result is the set of equations,

$$\mathbf{A}(\hat{\Omega})\zeta(\hat{\Omega}) - \mathbf{F}_s\boldsymbol{\phi} - \mathbf{s} + \sum_\gamma \mathbf{E}_\gamma(\hat{\Omega})\boldsymbol{\chi}_\gamma = 0 \ , \tag{14}$$

which can be solved for $\zeta(\hat{\Omega})$ to obtain

$$\zeta(\hat{\Omega}) = \mathbf{A}^{-1}(\hat{\Omega})\mathbf{F}_s\boldsymbol{\phi} + \mathbf{A}^{-1}(\hat{\Omega})\mathbf{s} - \sum_\gamma \mathbf{A}^{-1}(\hat{\Omega})\mathbf{E}_\gamma(\hat{\Omega})\boldsymbol{\chi}_\gamma \ . \tag{15}$$

We next integrate Eq. (15) over the angular domain and make use of the definition of the scalar flux in Eq. (5) to arrive at

$$\boldsymbol{\phi} = \mathbf{H}\mathbf{F}_s\boldsymbol{\phi} + \mathbf{H}\mathbf{s} - \sum_\gamma \mathbf{M}_\gamma\boldsymbol{\chi}_\gamma \ , \tag{16}$$

where

$$\mathbf{H} = \int d\Omega \, \mathbf{A}^{-1}(\hat{\Omega}) \tag{17}$$

and

$$\mathbf{M}_\gamma = \int d\Omega \, \mathbf{A}^{-1}(\hat{\Omega})\mathbf{E}_\gamma(\hat{\Omega}) \ . \tag{18}$$

Solving Eq. (16) for $\boldsymbol{\phi}$ yields the scalar flux distribution within the node,

$$\phi = \mathbf{Z}\mathbf{H}\mathbf{s} - \sum_\gamma \mathbf{Z}\mathbf{M}_\gamma\boldsymbol{\chi}_\gamma \ , \tag{19}$$

where

$$\mathbf{Z} = (\mathbf{I} - \mathbf{H}\mathbf{F}_s)^{-1} \tag{20}$$

$\mathbf{I}$ = identity matrix.

We use Eq. (19) to eliminate the scalar flux in Eq. (15) and obtain a relation for the even-parity flux explicitly in terms of the group source $\mathbf{s}$ and Lagrange multiplier coefficients, $\boldsymbol{\chi}_\gamma$:

$$\zeta(\hat{\Omega}) = [\mathbf{A}^{-1}(\hat{\Omega})(\mathbf{F}_s\mathbf{Z}\mathbf{H} + \mathbf{I})]\mathbf{s} - \sum_\gamma [\mathbf{A}^{-1}(\hat{\Omega})(\mathbf{F}_s\mathbf{Z}\mathbf{M}_\gamma + \mathbf{E}_\gamma(\hat{\Omega}))]\boldsymbol{\chi}_\gamma \ . \tag{21}$$

To complete the derivation, we utilize the continuity conditions at the interface imposed by the Lagrange multipliers. We first insert Eq. (7), the reduced nodal functional, into Eq. (1). Requiring this new equation to be stationary with respect to variations in $\boldsymbol{\chi}_\gamma$ yields the condition that the even-parity flux moments defined by

$$\boldsymbol{\Psi}_\gamma = \int d\Omega\, \mathbf{E}_\gamma^T(\hat{\Omega})\zeta(\hat{\Omega}) \tag{22}$$

be continuous across nodal interfaces. Upon substitution of Eq. (21) into Eq. (22), we obtain Eq. (23), which expresses the even-parity interface moments in terms of the group source and Lagrange multiplier, $\boldsymbol{\chi}_\gamma$:

$$\boldsymbol{\Psi}_\gamma = \mathbf{M}_\gamma^T(\mathbf{F}_s\mathbf{Z}\mathbf{H} + \mathbf{I})\mathbf{s} - \sum_{\gamma'}(\mathbf{M}_\gamma^T\mathbf{F}_s\mathbf{Z}\mathbf{M}_{\gamma'} + \mathbf{L}_{\gamma,\gamma'})\boldsymbol{\chi}_{\gamma'} \ , \tag{23}$$

where

$$\mathbf{L}_{\gamma,\gamma'} = \int d\Omega\, \mathbf{E}_\gamma^T(\hat{\Omega})\mathbf{A}^{-1}(\hat{\Omega})\mathbf{E}_{\gamma'}(\hat{\Omega}) \ . \tag{24}$$

We simplify Eq. (23) to a more compact form that is analogous to the spherical harmonics form implemented in VARIANT (Ref. 4):

$$\boldsymbol{\Psi}_\gamma = \mathbf{C}_\gamma\mathbf{s} - \sum_{\gamma'}\mathbf{G}_{\gamma,\gamma'}\boldsymbol{\chi}_{\gamma'} \ , \tag{25}$$

$$\mathbf{C}_\gamma = \mathbf{M}_\gamma^T(\mathbf{F}_s\mathbf{Z}\mathbf{H} + \mathbf{I}) \ , \tag{26}$$

and

$$\mathbf{G}_{\gamma,\gamma'} = \mathbf{M}_\gamma^T\mathbf{F}_s\mathbf{Z}\mathbf{M}_{\gamma'} + \mathbf{L}_{\gamma,\gamma'} \ . \tag{27}$$

Utilizing partitioned matrix notation, we may write the set of equations given by Eq. (25) as

$$\boldsymbol{\Psi} = \mathbf{C}\mathbf{s} - \mathbf{G}\boldsymbol{\chi} \ , \tag{28}$$

where the $\boldsymbol{\Psi}$ and $\boldsymbol{\chi}$ vectors now include all of the node interfaces. To express this result in conventional response matrix notation, we introduce the partial current-like variables

$$\mathbf{j}^{\pm} = \tfrac{1}{4}\boldsymbol{\Psi} \pm \tfrac{1}{2}\boldsymbol{\chi} \tag{29}$$

along the node interfaces. Combining Eqs. (28) and (29) leads to the response matrix equation

$$\mathbf{j}^{+} = \mathbf{B}\mathbf{s} + \mathbf{R}\mathbf{j}^{-} \ , \tag{30}$$

where

$$\mathbf{R} = (\tfrac{1}{2}\mathbf{G} + \mathbf{I})^{-1}(\tfrac{1}{2}\mathbf{G} - \mathbf{I}) \tag{31}$$

and

$$\mathbf{B} = (\tfrac{1}{2}\mathbf{G} + \mathbf{I})^{-1}(\tfrac{1}{2}\mathbf{C}) \ . \tag{32}$$

A distinct characteristic of the forgoing derivation is the appearance of $\mathbf{A}^{-1}(\hat{\Omega})$ in the integrands of Eqs. (17), (18), and (24). Since the analytic inversion of $\mathbf{A}(\hat{\Omega})$ is impractical, we evaluate the angular integrals numerically using a standard Gaussian quadrature integration scheme. Specifically, we implement a Legendre quadrature in the polar direction and a Chebychev quadrature in the azimuthal direction. Using *n* order Legendre and Chebychev approximations over an octant of the unit sphere, we obtain a "square" Legendre-Chebychev (SLC) product quadrature: an SLC_n quadrature. For odd-parity interface expansions of order *N*, a minimum SLC_{N+3} quadrature is required to produce accurate integrals. In Sec. III an SLC_{16} quadrature is used for all three benchmarks, resulting in 128 integration points.

III. RESULTS

Response matrix equations based on the integral formulation derived in Sec. II have been implemented as two sets of modifications of the VARIANT code. Each replaces the even-parity spherical harmonics expansion with the integral approach, but retains the existing iterative solution algorithms as well as most of the data structures and other code characteristics. In the first, VARIANT-I, the integral method is applied using the orthogonal spatial polynomial trial functions already available in VARIANT; it is thus suitable for problems with homogeneous nodes. In the second, VARIANT-ISE, the integral method is employed in conjunction with the finite subelement (SE) method of earlier work.[9]

We solve three benchmark problems in *x-y* geometry to examine the capabilities of the integral method. The first benchmark, due to Azmy,[12] is a fixed-source deep-penetration problem, and the second is a criticality calculation specified by Wagner.[13] Since both of these problems utilize homogeneous nodes, we compare VARIANT-I to the production form of VARIANT. We employ sixth-order spatial polynomial approximations for the even-parity flux and group source, and quadratic Lagrange multipliers at the node interfaces in all calculations for both benchmarks, thereby eliminating differences caused by the spatial approximations. The third problem is the two-dimensional form of the recent OECD/Nuclear Energy Agency (NEA) MOX core benchmark.[14] For it, we compare results obtained using VARIANT-SE and VARIANT-ISE to a reference Monte Carlo solution. For the MOX benchmark we define each node to correspond to a single pin cell and implement identical finite element and Lagrange multiplier approximations to eliminate discrepancies caused by different spatial treatments.[9] We first examine the accuracy of the results for the three benchmarks and then discuss the impact of the integral formulation on CPU times and memory requirements.

III.A. One-Group Fixed-Source Benchmark

The layout for the Azmy benchmark problem[12] is shown in Fig. 1, while the cross-section and source data are given in Table I. The computational objective specified for this benchmark is to obtain the scalar flux distribution along the line (9.84375, *y*) as indicated in Fig. 1. The flux solutions are shown in Fig. 2 for both VARIANT

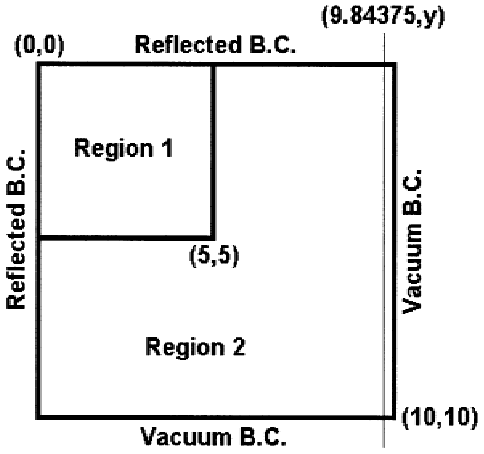

Fig. 1. Azmy benchmark geometry.

TABLE I

Cross Section and Source Data for the AZMY Benchmark

Region	Total	Absorption	Scattering	Isotropic Source
1	1.0	0.5	0.5	1.0
2	2.0	1.9	0.1	0.0

and VARIANT-I with P_1, P_3, and P_{11} interface approximations. Also included in Fig. 2 are reproductions of the TWODANT (Ref. 15) S_4 and S_{16} angular approximations using the mesh specified in Ref. 12. The VARIANT P_{11} solution is taken to be the reference since further refinement of the space-angle approximation yielded negligible improvement in the solution. Although the P_1 solutions of both VARIANT and VARIANT-I display large errors, the VARIANT-I flux distribution is significantly more accurate than that of VARIANT. Likewise, while substantial error remains in the VARIANT P_3 solution, the VARIANT-I P_3 solution is nearly indistinguishable from the reference P_{11} solution. Thus, for fixed-source problems of this nature, replacing the standard P_N nodal method with the integral treatment offers significant potential. The TWODANT solutions clearly display the ray effect phenomena common to discrete ordinate methods for problems such as this. With a higher-order angular quadrature in TWODANT, one would expect the solution to converge closer to that of the VARIANT reference.

III.B. Two-Group Eigenvalue Benchmark

The configuration for the Wagner two-group criticality benchmark[14] is given in Fig. 3 and the cross sections in Table II. The benchmark specifies reflected boundary conditions on all surfaces, hereafter called problem 1. To accentuate transport effects, we also

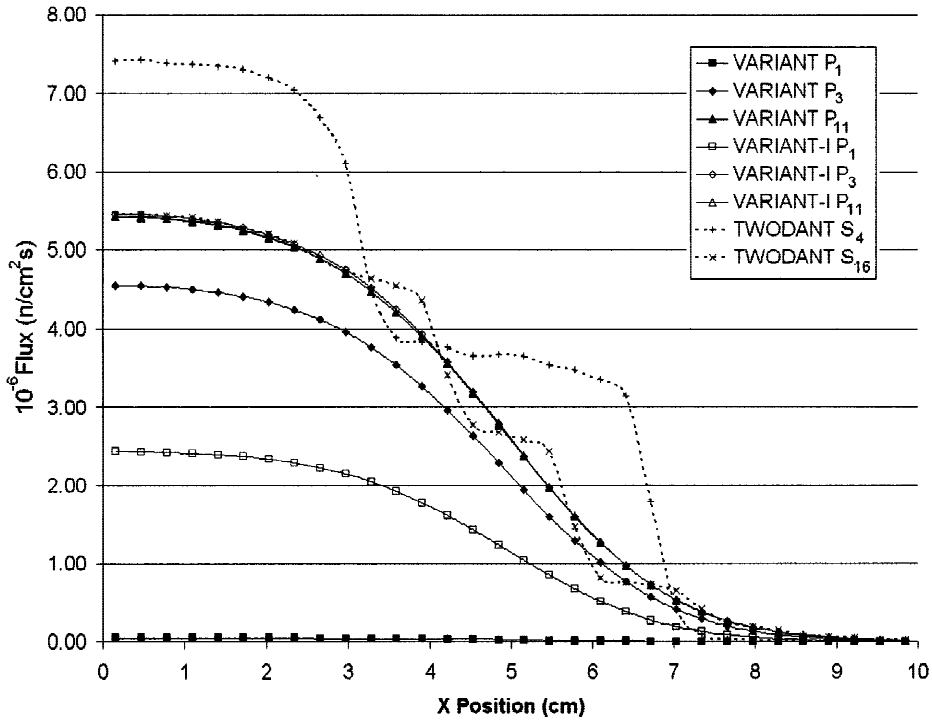

Fig. 2. Azmy benchmark VARIANT, VARIANT-ISE, and TWODANT solutions.

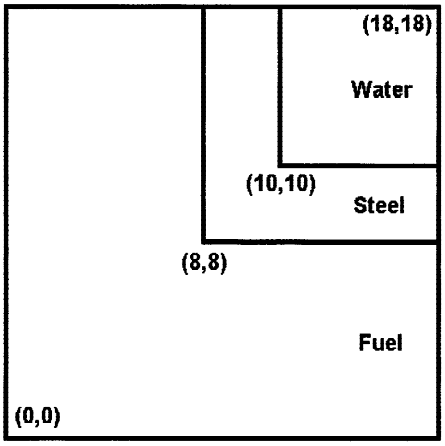

Fig. 3. Two-group benchmark geometry.

TABLE II

Two-Group Benchmark Cross Sections

Cross Section	Fuel Composition		Steel Composition		Water Composition	
	1	2	1	2	1	2
S_a	0.01	0.07	0.003	0.11	0.001	0.03
χS_f	0.006	0.1	0.0	0.0	0.0	0.0
S_t	0.22	0.8	0.53	0.94	0.701	2.0
$S_{1\chi 2}$		0.017		0.001		0.05
S_s	0.193	0.73	0.526	0.83	0.65	1.97
χ	1.0	0.0				

include results for a modified configuration (problem 2) with vacuum boundary conditions at the top and right, and reflected boundary conditions at the bottom and left. A P_{17}, eighth-order spatial flux and source, and cubic spatial leakage approximation were implemented in VARIANT to obtain reference eigenvalue solutions of 0.901504 for problem 1 and 0.645602 for problem 2. Table III provides percent error data for the VARIANT and VARIANT-I codes using a sixth-order spatial flux and source approximation and quadratic spatial leakage. The TWODANT solutions are for S_{N+1} quadratures where N represents the angular order of the P_N approximation used (i.e., S_2, S_4, S_6, S_8,...). Table III indicates clear convergence toward the reference solution for all three transport codes. However, there appears to be some residual error remaining in the solutions, and additional calculations were performed using TWODANT and VARIANT-I to resolve these discrepancies. For VARIANT-I, refinements of the space-angle approximations cut the error for problems 1 and 2 to 0.0040 and 0.0316%, respectively, but did not account fully for the discrepancies seen. Refinements of the spatial mesh and angular quadrature in TWODANT actually increased the error for problems 1 and 2 to 0.0105 and 0.0362%, respectively. Given that further refinements of the space-angle variables do not account for the remaining discrepancies, one must attribute the small remaining differences to the nuances between formulations.

III.C. Seven-Group MOX Small-Core Benchmark

The seven-group MOX small-core problem specified by OECD/NEA (Ref. 14) is shown in Fig. 4. Each pin is 1.08 cm in diameter, each square is 1.26 cm in length, and the moderator region is 21.42 cm thick. Seven-group cross sections for each of the compositions defined in Fig. 4 were included in the benchmark specification. A reference solution obtained with an MCNP (Ref. 16) multigroup Monte Carlo calculation yields an eigenvalue of 1.18655, with a 68% confidence interval of $\pm 0.0034\%$, and estimates of all of the pin powers with associated statistical errors.

TABLE III

Eigenvalue Percent Error Data for VARIANT, VARIANT-I, and TWODANT for the Two-Group Benchmark

N	Problem 1			Problem 2		
	VARIANT	VARIANT-I	TWODANT $(N+1)$	VARIANT	VARIANT-I	TWODANT $(N+1)$
1	−1.0268	0.2473	−0.8366	−2.0659	0.7044	−1.3991
3	−0.0565	0.0364	0.1996	−0.1805	0.2187	0.3241
5	−0.0142	0.0156	0.0664	−0.0688	0.1286	0.1237
7	−0.0056	0.0096	0.0242	−0.0342	0.0940	0.0686
9	−0.0022	0.0071	0.0067	−0.0181	0.0753	0.0457
11	−0.0004	0.0058	−0.0023	−0.0090	0.0639	0.0337

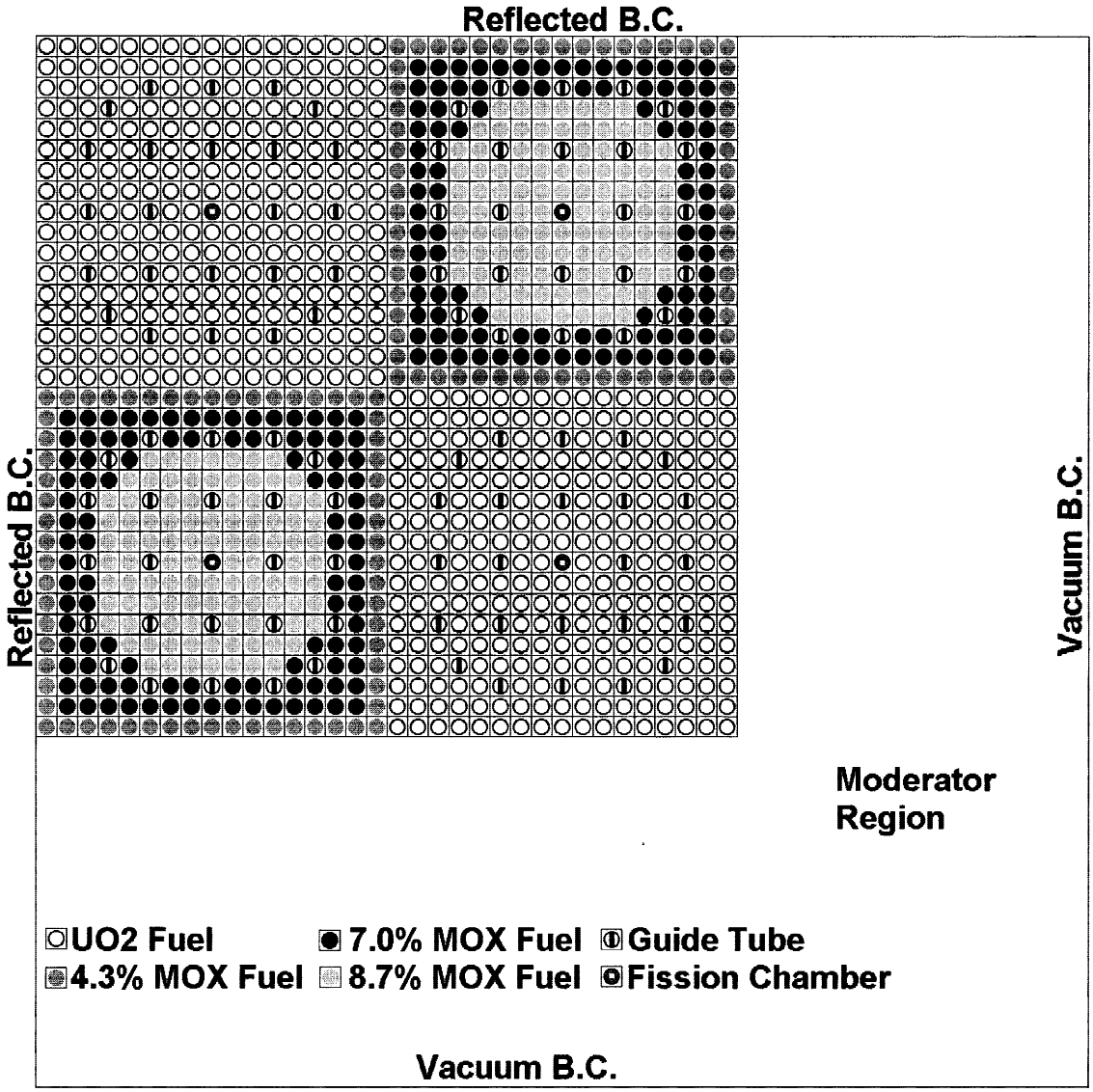

Fig. 4. The benchmark core configuration.

In earlier work, extensive studies of this benchmark were performed using the subelement technique coupled to the standard spherical harmonics formulation referred to here as VARIANT-SE (Refs. 8 and 9). Here, we compare VARIANT-SE and VARIANT-ISE results using the quadratic finite element mesh in Fig. 5 to represent each fuel pin cell. Our sensitivity studies indicated that spatial mesh truncation errors are insignificant when this subelement grid is combined with cubic Lagrange multiplier approximations at the node interfaces. In this work we utilize four error measures to examine the accuracy of the VARIANT-SE and VARIANT-ISE solutions: the eigenvalue percent error (Eigenvalue), the percent error of the pin with the maximum power (Maximum Pin Power), the maximum percent error of all of

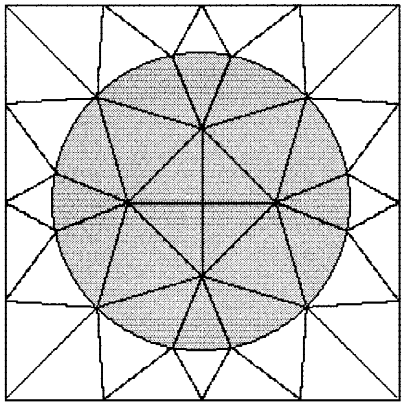

Fig. 5. Finite element mesh approximation.

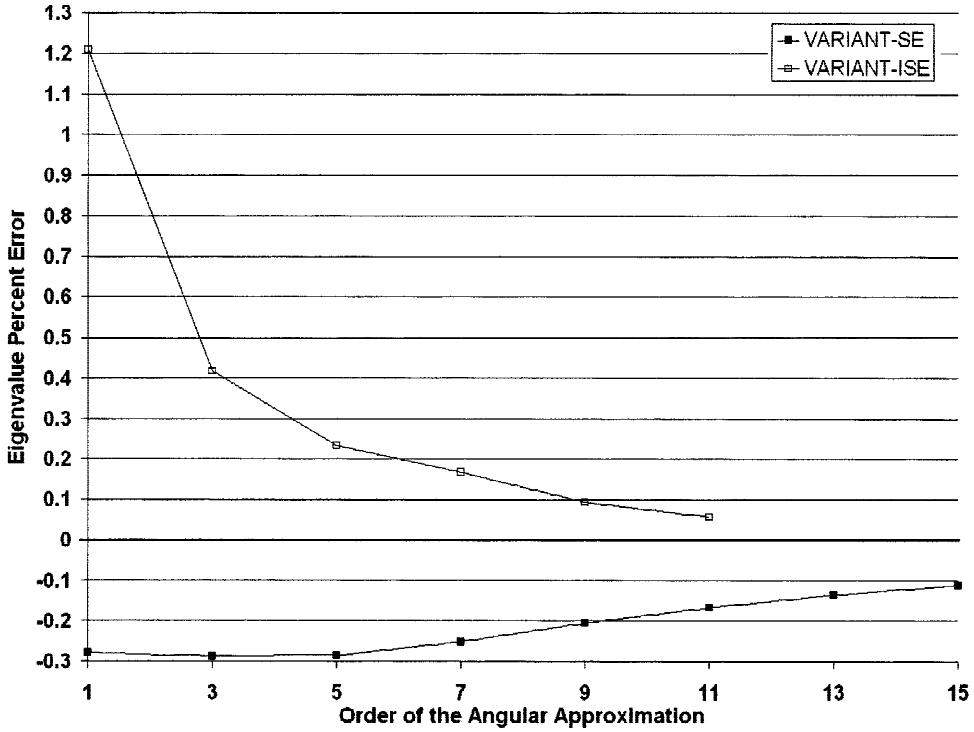

Fig. 6. VARIANT-SE and VARIANT-ISE solutions for the seven-group benchmark.

the fuel pins (Maximum), and the root-mean-square of the pin power percent error distribution (RMS). Figure 6 shows the eigenvalue percent error trend for the two codes while Table IV provides tabulated results for all four error measures. The ± Monte Carlo values in Table IV represent the 99% confidence intervals for the MCNP reference calculation.

Figure 6 and Table IV indicate that both the spherical harmonic and integral approaches converge toward the Monte Carlo solution as the angular approximation at the interface is refined. The integral method yields less accurate eigenvalue results for low-order interface conditions, but with interface orders higher than P_5, which are typically required for cellular problems of

TABLE IV

VARIANT-SE and VARIANT-ISE Percent Error Measures

	Eigenvalue		Maximum Pin Power		Maximum		RMS	
Angular Order	SE	ISE	SE	ISE	SE	ISE	SE	ISE
P_1	−0.278	1.209	0.942	2.818	5.911	10.579	1.726	2.077
P_3	−0.287	0.419	1.348	0.861	2.259	1.585	1.023	0.672
P_5	−0.286	0.233	0.995	0.413	1.797	0.975	0.763	0.363
P_7	−0.250	0.167	0.751	0.249	1.532	0.747	0.588	0.253
P_9	−0.205	0.092	0.583	0.086	1.345	0.526	0.470	0.176
P_{11}	−0.166	0.057	0.468	0.012	1.214	0.593	0.393	0.162
MCNP	±0.008		±0.16		±0.58		±0.36	

this nature, the integral treatment of VARIANT-ISE is significantly more accurate than VARIANT-SE. This trend is even more pronounced in the pin power results.

III.D. Computational Comparisons

The benchmark results presented above indicate that the integral form of the variational nodal method produces results of comparable or superior accuracy to those of the spherical harmonics treatment. The differences are attributable wholly to the integral treatment of the even-parity flux since in all cases comparisons are made utilizing identical spatial trial functions and the same order odd-parity spherical harmonics expansions along the node interfaces. The greatest accuracy enhancements tend to appear in those calculations requiring very high-order angular approximations, such as the MOX core benchmark treated in Sec. III.C. We have also found that in such high-order transport calculations, the integral formulation of VARIANT-ISE enables considerable reductions in both memory requirements and CPU times relative to those required for VARIANT-SE. These reductions may be explained as follows, using the Cartesian *x-y* geometry of the foregoing MOX benchmark as an example.

Variational nodal calculations are performed in two steps: (a) formation of the nodal response matrices and (b) iterative solution of the resulting response matrix equations. The most prominent difference between the integral treatment and the spherical harmonics treatment appears in the response matrix formation. Let S be the number of spatial degrees of freedom utilized to approximate the even-parity flux within the node and T be the number of spatial degrees of freedom utilized in the Lagrange multiplier approximation for each nodal surface. For the MOX benchmark problem, which utilizes the finite element mesh shown in Fig. 5, $S = 113$ and $T = 4$. An N'th order spherical harmonics expansion has $\frac{1}{4}(N + 1)^2$ even-parity moments that are coupled to the internal spatial approximation. Thus, to obtain a response matrix using the spherical harmonic treatment, the inversion of a banded symmetric coefficient matrix of dimension $\frac{1}{4}S(N + 1)^2$ must be carried out. This matrix represents the bulk of the memory requirement and computational time needed to obtain a response matrix for the VARIANT-SE treatment. In contrast, for the integral treatment of VARIANT-ISE, $\mathbf{A}(\hat{\Omega})$ with dimension S is the largest matrix to be inverted for low-order angular interface approximations while $\mathbf{G}$, with dimension $T(N + 3)(N + 1)$, dominates at high-order angular interface approximations. However, since $\mathbf{A}(\hat{\Omega})$ must be inverted 128 times (the number of integration points in the SLC_{16} quadrature), it accounts for the majority of the CPU

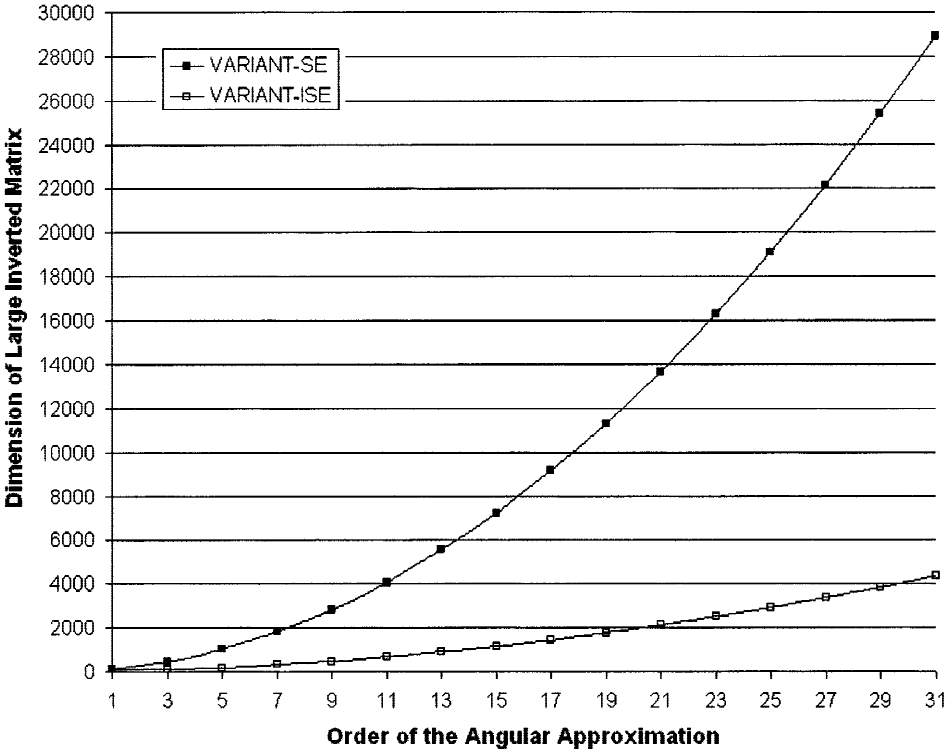

Fig. 7. Dimensions of largest inverted matrix for the Q2 mesh, cubic Lagrange multiplier response matrix calculation.

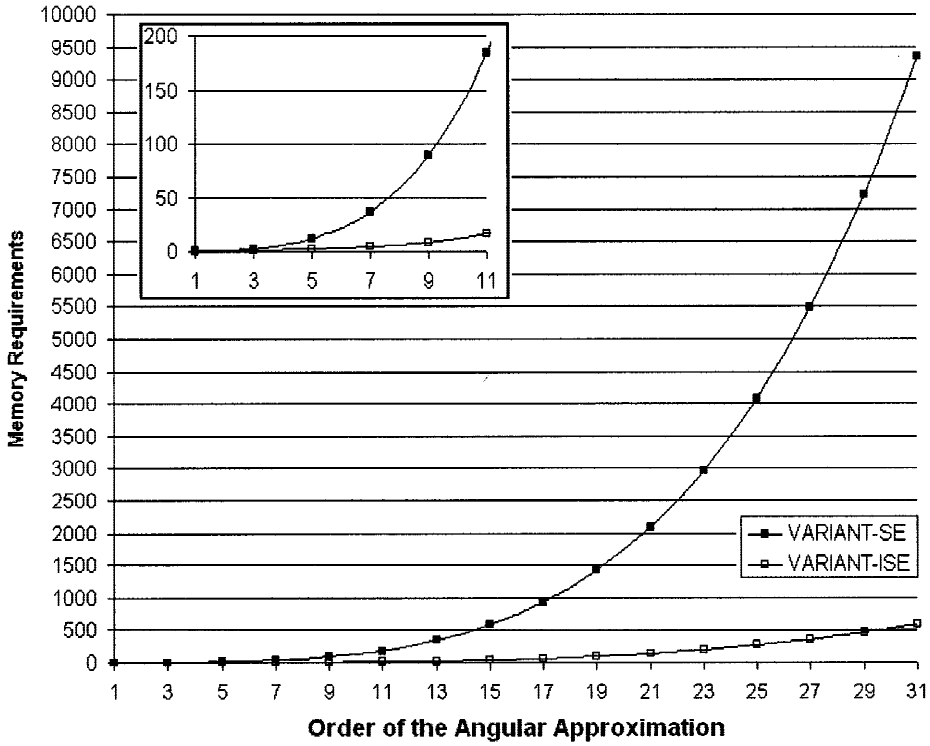

Fig. 8. Total memory (MB) for the Q2 mesh, cubic Lagrange multiplier response matrix calculation.

time in the response matrix formation for the integral method.

For problems utilizing high-order odd-parity spherical harmonics expansions along the node interfaces, the differences in memory requirements and computational times for the spherical harmonic and integral response matrix formulations become quite dramatic. In Fig. 7 we have plotted the dimension of the largest inverted matrix for the two approaches as a function of the interface angular approximation. Similarly, in Fig. 8 we have plotted the total memory requirements for the two methods as a function of interface angular approximation.

The integral response matrices formed in VARIANT-SE have slightly smaller dimensions because of the removal of the $(N+1)/2$ terms from the angular interface expansions. While this increases the memory requirements and running time for the iterative solution algorithm in VARIANT-ISE, the net effect is minor compared to the savings incurred in response matrix formation. Table V displays the net effects on memory requirements and CPU time for the MOX benchmark problem for different levels of interface approximation.

TABLE V

CPU Time and Total Memory Ratios
(VARIANT-ISE/VARIANT-SE)

	CPU Time	Memory
P_1	1.433	2.503
P_3	1.366	0.427
P_5	1.120	0.181
P_7	1.112	0.121
P_9	0.685	0.098
P_{11}	0.502	0.086

IV. CONCLUSIONS

An integral form of the variational nodal method has been presented, utilizing both orthogonal polynomial and finite subelement approximation treatments of the spatial variables. A two-dimensional implementation of the integral method in the VARIANT code has been carried out, and the new method tested on three benchmark problems. The first benchmark demonstrated the method's ability to obtain the flux solution for a fixed-source deep-penetration problem, while the second demonstrated its ability to solve simple criticality problems. The third benchmark, by far the most difficult, illustrated the method's capability for treating situations in which lattice effects combined with sharp global flux gradients to require very high order angular approximations throughout the problem domain.

For calculations requiring higher-order angular approximations, the integral method yields solutions with favorable accuracy compared to those obtained using the standard spherical harmonics approach. Moreover, for such calculations the integral method requires dramatically less CPU time and memory than the spherical harmonics approach. Such results encourage consideration for extending the integral formulation to wider classes of problems; these would include hexagonal and Cartesian three-dimensional geometries and problems that include anisotropic scattering. Opportunities also remain for improving algorithms and optimizing coding to reduce the CPU and memory burdens imposed by large transport computations.

ACKNOWLEDGMENTS

This work is based, in part, on a dissertation submitted by the first author in partial fulfillment of the PhD requirements at the University of Missouri-Rolla. It was supported by the U.S. Department of Energy under contract W-31-109-ENG-38 and by the U.S. Department of Energy under contract DE-FG07-98ID13632.

REFERENCES

1. D. LAWRENCE, "Progress in Nodal Methods for the Solution of the Neutron Diffusion and Transport Equations," *Prog. Nucl. Energy*, **17**, 271 (1986).

2. M. R. WAGNER, "Three-Dimensional Nodal Diffusion and Transport Theory for Hexagonal-*z* Geometry," *Nucl. Sci. Eng.*, **103**, 377 (1989).

3. C. B. CARRICO, E. E. LEWIS, and G. PALMIOTTI, "Three Dimensional Variational Nodal Transport Methods for Cartesian, Triangular, and Hexagonal Criticality Calculations," *Nucl. Sci. Eng.*, **111**, 168 (1992).

4. G. PALMIOTTI, E. E. LEWIS, and C. B. CARRICO, "VARIANT: VARIational Anisotropic Nodal Transport for Multidimensional Cartesian and Hexagonal Geometry Calculation," ANL-95/40, Argonne National Laboratory (1995).

5. M. A. SMITH, N. TSOULFANIDIS, G. PALMIOTTI, T. A. TAIWO, and E. E. LEWIS, "Higher Order Angular Capabilities of the VARIANT Code," *Trans. Am. Nucl. Soc.*, **86**, 321 (2002).

6. T. H. FANNING and G. PALMIOTTI, "Variational Nodal Transport Methods with Heterogeneous Nodes," *Nucl. Sci. Eng.*, **127**, 154 (1997).

7. E. E. LEWIS, G. PALMIOTTI, and T. TAIWO, "Space-Angle Approximations in the Variational Nodal Method," *Proc. Int. Conf. Mathematics and Computations, Reactor Analysis and Environmental Analysis in Nuclear Applications*, Madrid, Spain, September 27–30, 1999, Vol. 1, p. 827 (1999).

8. M. A. SMITH, "Implementation of the Finite Element Approximation in a Nodal Three-Dimensional Transport Program to Allow for Explicit Node Geometries," PhD Dissertation, University of Missouri-Rolla (2001).

9. M. A. SMITH, N. TSOULFANIDIS, E. E. LEWIS, G. PALMIOTTI, and T. A. TAIWO, "A Finite Element Generalization of the Variational Nodal Method," *Nucl. Sci. Eng.*, **144**, 36 (2003).

10. E. E. LEWIS, W. F. MILLER, Jr., and T. P. HENRY, "A Two-Dimensional Finite Element Method for Integral Neutron Transport Calculations," *Nucl. Sci. Eng.*, **58**, 202 (1975).

11. E. E. LEWIS, C. B. CARRICO, and G. PALMIOTTI, "Variational Nodal Formulation for the Spherical Harmonics Equations," *Nucl. Sci. Eng.*, **122**, 194 (1996).

12. Y. Y. AZMY, "The Weighted Diamond-Difference Form of Nodal Transport Methods," *Nucl. Sci. Eng.*, **98**, 29 (1988).

13. M. R. WAGNER, "A Nodal Discrete-Ordinates Method for the Numerical Solution of the Multidimensional Transport Equation," *Proc. Topl. Mtg. Computational Methods in Nuclear Engineering*, Williamsburg, Virginia, April 23–25, 1979, Vol. II, p. 4-117, American Nuclear Society (1979).

14. E. E. LEWIS, G. PALMIOTTI, T. A. TAIWO, R. N. BLOMQUIST, M. A. SMITH, and N. TSOULFANIDIS, "Benchmark Specification for Deterministic 2-D/3-D MOX Fuel Assembly Transport Calculations Without Spatial Homogenization (C5G7 MOX)," NEA/NSC/DOC(2001)4, Nuclear Energy Agency (Mar. 2001).

15. R. E. ALCOUFFE, F. W. BRINKLEY, D. R. MARR, and R. D. O'DELL, "User's Guide for TWODANT: A Code Package for Two-Dimensional, Diffusion-Accelerated Neutral Particle Transport," LA-10049-M, Los Alamos National Laboratory (1984).

16. "MCNP—A General Monte Carlo N-Particle Transport Code," LA-12625-M, J. F. BRIESMEISTER, Ed., Los Alamos National Laboratory (Mar. 1997).